Draft version September 21, 2018
Typeset using LaTeX **twocolumn** style in AASTeX62

Predicting the Rossby number in convective experiments

Evan H. Anders,[1,2] Cathryn M. Manduca,[2] Benjamin P. Brown,[1,2] Jeffrey S. Oishi,[3] and Geoff Vasil[4]

[1] *Dept. Astrophysical & Planetary Sciences, University of Colorado – Boulder, Boulder, CO 80309, USA*
[2] *Laboratory for Atmospheric and Space Physics, Boulder, CO 80303, USA*
[3] *Department of Physics and Astronomy, Bates College, Lewiston, ME 04240, USA*
[4] *University of Sydney School of Mathematics and Statistics, Sydney, NSW 2006, Australia*

(Received September 21, 2018; Revised September 21, 2018; Accepted September 21, 2018)

Submitted to ApJ

ABSTRACT

In this letter we study numerical simulations of stratified, compressible convection in a rotational f-plane geometry. We define a new quantity, the Predictive Rossby number ($\mathcal{P}_{\rm Ro}$), and show that it specifies the evolved Rossby number (Ro) of a convective simulation. We examine the scaling of traditional fluid numbers and boundary layers along paths of constant $\mathcal{P}_{\rm Ro}$.

Keywords: convection — rotation — turbulence

1. INTRODUCTION

Convective flows in stars and planets are influenced by rotation. Rotating convection has been studied in great detail in recent decades in both laboratory and numerical settings. The properties of convection in the regime in which rotational forces are insignificant are now well understood (King et al. 2009; Zhong et al. 2009; Cheng et al. 2015). Boussinesq convective theory is also robust in the rapidly rotating regime (Julien et al. 2012; Stellmach et al. 2014; Gastine et al. 2016). We are not, however, aware of any well-developed procedure for specifying the degree of rotational constraint in a convective experiment *a priori*. Rather, the rotational constraint, measured by the evolved Rossby number (Ro, the ratio of advective dynamics to rotational constraint), is a complex combination of input parameters, such as convective driving and the magnitude of the rotation vector.

A vast number of studies of rotating convection have been conducted in the astrophysical context. Often these studies focus on questions inspired by the solar dynamo (Glatzmaier & Gilman 1982; Busse 2002; Brown et al. 2008, 2010, 2011; Augustson et al. 2012; Guerrero et al. 2013; Käpylä et al. 2014). Even when these simulations appear to be rotating at a rate similar to the Sun, they can produce vastly different dynamics (such as anti-solar differential rotation). These strange results may be the result of these systems having different evolved values of the Rossby number than the Sun. Recent simulations and experiments are predicting that the Rossby number of the deep interior of the Sun is low, and that this drastically affects the behavior of the dynamics of the solar convection zone (Featherstone & Hindman 2016; Greer et al. 2016).

In addition to it being very important to study the correct Rossby number regime in solar convection studies, it also seems to be very important in studies of planetary dynamos. For example, the balance between Lorentz forces and rotational forces likely creates the observed differences between ice giant and gas giant dynamos in our solar system (Soderlund et al. 2015). Furthermore, Aurnou & King (2017) suggest that many studies in planetary systems have likely over-emphasized the importance of magnetism compared to rotation.

It is clear that in studying astrophysical objects, the experimenter must study the proper Rossby number regime, and thus the proper degree of rotational constraint. In this work, our goal is to find a way of specifying the Rossby number of convection in a simplified system through changing the input parameters. In Anders & Brown (2017) (hereafter AB17), we studied non-rotating, hydrodynamic, compressible convection in polytropic atmospheres. In this work, we extend the study of AB17 to rotationally-influenced, f-plane

Corresponding author: Evan H. Anders
evan.anders@colorado.edu

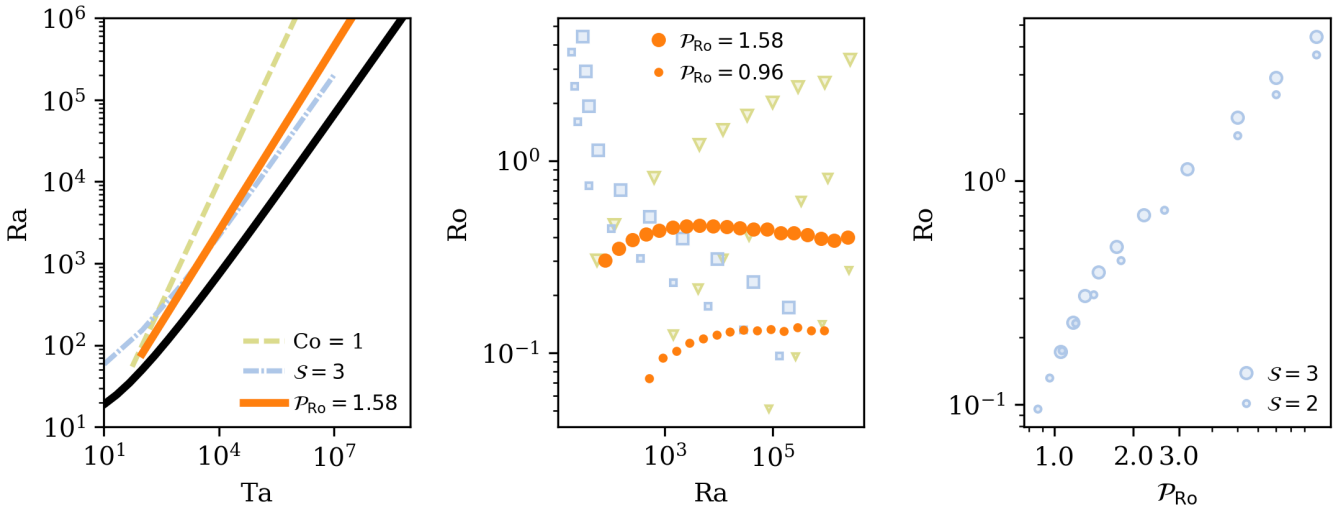

Figure 1. (a) The critical Rayleigh number, as a function of the Taylor number, is plotted as a solid black line. Paths of constant Convective Rossby Number (red dashed line), constant supercriticality (orange dashed line), and $\mathcal{P}_{\rm Ro}$ (blue solid line) are shown through parameter space. (b) Evolved Ro is plotted vs. Ra along multiple constant $\mathcal{P}_{\rm Ro}$ paths and the constant Co and $\mathcal{S}$ path shown in (a). After a sharp increase at low Ta, the evolved Rossby number flattens out and stays nearly constant across orders of magnitude of Ta. (c) At low Ro, we find that Ro $\propto \mathcal{P}_{\rm Ro}{}^{X}$.

atmospheres, as have been previously studied by e.g., Brummell et al. (1996, 1998); Calkins et al. (2015). Our goal is to determine how the input parameters which we studied previously (which control the Mach number and Reynolds number of the evolved flows) couple with a new input parameter, the Taylor number (Ta, Julien et al. (1996)), which sets the magnitude of the rotational vector.

In section 2, we describe our atmosphere, numerical experiment, and paths through parameter space. In section 3, we present the results of our experiments and in section 4 we offer concluding remarks.

2. EXPERIMENT

We study fully compressible, stratified convection under precisely the same atmospheric model as we previously did in AB17, and here we have included rotation. We study polytropic atmospheres with $n_\rho = 3$ density scale heights and a superadiabatic excess of $\epsilon = 10^{-4}$ such that flows are at low Mach number. As in previous work (Julien et al. 1996; Brummell et al. 1996), we study a domain in which the gravity, $\boldsymbol{g} = -g\hat{z}$, and rotational vector, $\boldsymbol{\Omega} = \Omega\hat{z}$, are antiparallel.

We evolve the velocity ($\boldsymbol{u}$), temperature (T), and log density ($\ln\rho$) according to the Fully Compressible Navier-Stokes equations in the same form presented in AB17, with the addition of the Coriolis term, $2\boldsymbol{\Omega} \times \boldsymbol{u}$, to the left-hand side of the momentum equation. We impose impenetrable, stress-free, fixed-temperature boundary conditions at the top and bottom of the domain.

The kinematic viscosity (ν), thermal diffusivity (χ), and strength of rotation (Ω) are set at the top of the domain by the Rayleigh number (Ra), Prandtl number (Pr), and Taylor number (Ta),

$$\mathrm{Ra} = \frac{gL_z^3\Delta S/c_P}{\nu\chi}, \quad \mathrm{Pr} = \frac{\nu}{\chi}, \quad \mathrm{Ta} = \left(\frac{2\Omega L_z^2}{\nu}\right)^2, \qquad (1)$$

where L_z is the depth of the domain, $\Delta S = \epsilon n_\rho/m$ is the specific entropy difference between $z = 0$ and $z = L_z$, and the specific heat at constant pressure is c_P. Throughout this work we set Pr = 1.

As Ta increases, the wavenumber of convective onset, $k_{\rm crit}$, also increases (**?**). We study 3D cartesian convective domains with horizontal extents of $x, y = [0, 4(2\pi/k_{\rm crit})]$. We evolve our simulations using the Dedalus[1] pseudospectral framework, and our numerical methods are identical to those presented in AB17.

As Ta increases, the critical value of Ra at which convection onsets, $\mathrm{Ra}_{\rm crit}$, also increases (see the black line in Fig. 1a). The linked nature of these crucial control parameters makes it difficult to predict the rotational constraint of the evolved fluid flows for a given set of input parameters. In this work, we will explore three paths through Ra-Ta space:

$$\mathrm{Ra} = \begin{cases} \mathcal{S}\,\mathrm{Ra}_{\rm crit}(\mathrm{Ta}), & \text{(I)} \\ \mathrm{Co}^2\mathrm{Pr}\ \mathrm{Ta}, & \text{(II)} \\ \mathcal{P}_{\rm Ro}{}^2\mathrm{Pr}\ \mathrm{Ta}^{3/4} & \text{(III)}. \end{cases} \qquad (2)$$

[1] http://dedalus-project.org/

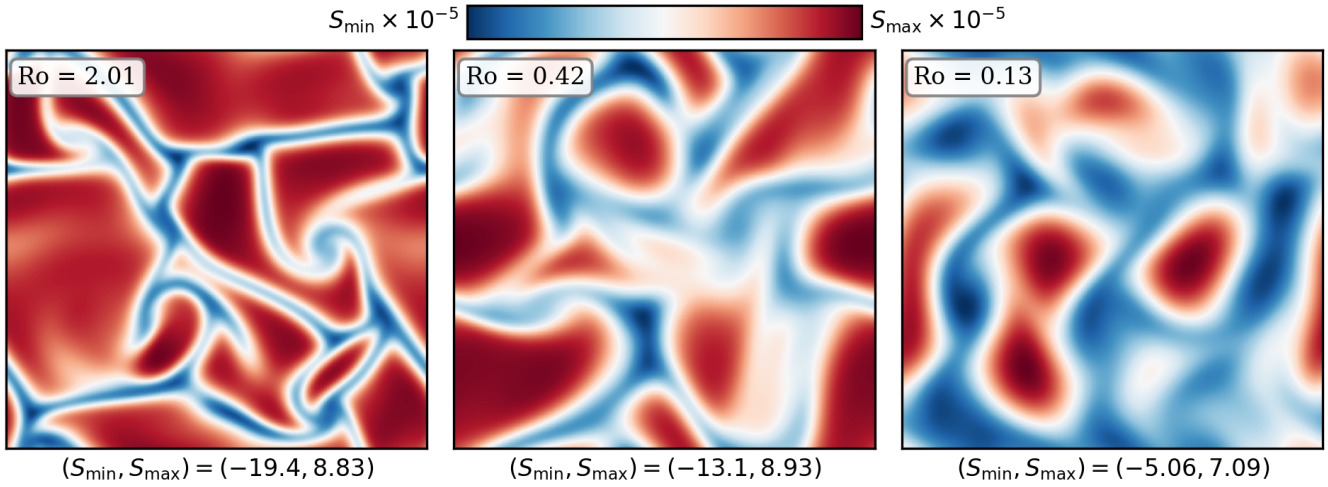

Figure 2. A horizontal slice of the evolved entropy field is plotted at $z = 0.95L_z$ for select simulations. The mean value of entropy at this height has been removed in all cases. All runs displayed here have an evolved volume-averaged Ro $\sim$ 200. As Ro decreases O(1) on the left to O(0.1) on the right, and thus the rotational constraint on the flow increases, significant changes in flow morphology are observed. At Ro = 2.01, convective dynamics are not hugely dissimilar from the non-rotating case where there are large upflows and narrow, fast downflow lanes (see e.g., AB17). As the rotational constraint increases, the granular convective pattern gives way to vortical columns, as seen at Ro = 0.13.

Paths on constraint I are at constant supercriticality, $\mathcal{S} \equiv \mathrm{Ra}/\mathrm{Ra}_{\mathrm{crit}}$ (blue dash-dot line in Fig. 1a). Paths on constraint II are at a constant value of the classic "Convective Rossby number" (Co = Ra / [Pr Ta]), which has been used frequently in past work, and is intended to predict the rotational constraint of the evolved solution (green dashed line in Fig. 1a; Julien et al. (1996); Brummell et al. (1996)). Paths on constraint III set constant a ratio which we call the "Predictive Rossby Number," ${\mathcal{P}_{\mathrm{Ro}}}^2 = \mathrm{Ra}/(\mathrm{PrTa}^{3/4})$, (e.g., orange solid line in Fig. 1a). To our knowledge, these paths have not been in the literature.

For each path defined in Eqn. 2, our goal is to study the magnitude of the rotational constraint as quantified by the Rossby number,

$$\mathrm{Ro} = \frac{|\nabla \times \boldsymbol{u}|}{2\Omega}. \tag{3}$$

If Ro remains constant over a large range of Ra along one of these paths, then studies in which the magnitude of Ro is important should conduct experiments along that path.

3. RESULTS & DISCUSSION

In Fig. 1a, the value of $\mathrm{Ra}_{\mathrm{crit}}$ is shown as a function of Ta, as calculated by a linear instability analysis. A sample path for each criterion in Eqn. 2 through this parameter space is shown. In Fig. 1b, we display the scaling of Ro with increasing Ra along various paths through parameter space. We find that Ro increases on constant Co paths, decreases on constant $\mathcal{S}$ paths, and remains roughly constant along constant $\mathcal{P}_{\mathrm{Ro}}$ paths. In Fig. 1c, the behavior of Ro is shown as a function of $\mathcal{P}_{\mathrm{Ro}}$ at constant $\mathcal{S}$. At low Ro and $\mathcal{P}_{\mathrm{Ro}}$, in the rotationally constrained regime, the two parameters are related according to the power law [INSERT HERE ONCE MORE DATA]. At higher Ro in the rotationally unconstrained regime, this scaling breaks down to a [INSERT SCALING], with some offset at different values of $\mathcal{S}$.

In Fig. 2, sample horizontal snapshots of the evolved entropy field near the top of the domain are shown. In Fig. 2a, a rotationally uncontrained flow at moderately high Ro is shown. In Figs. 2b&c, increasingly rotationally constrained convection is shown. As Ro decreases, the classic granular structure of convection (see e.g., Fig. 2 in AB17) gives way to vortical columns of convection, as seen in rapidly rotating Rayleigh-Bénard convection (Stellmach et al. 2014). The select cases displayed in Fig. 2 have an evolved volume-averaged Re $\sim$ 200.

We measure the Nusselt number (Nu, which quantifies heat transport in a convective solution) as we did in AB17. In Fig. 3a, we show how Nu scales as a function of Ra at fixed $\mathcal{P}_{\mathrm{Ro}}$. For constant $\mathcal{P}_{\mathrm{Ro}}$, we find a scaling of $\mathrm{Nu} \propto \mathrm{Ra}^{0.27}$ in the rotationally constrained regime. This is reminiscent of classic scaling laws in non-rotating Rayleigh-Bénard convection (**?**). This suggests that changes in heat transport at constant $\mathcal{P}_{\mathrm{Ro}}$ are driven by changes in the boundary layer structure with increasing Ra. In Fig. 3b, we plot the RMS Reynold's number ($\mathrm{Re} = |u|L_z/\nu$) as a function of Ra at fixed $\mathcal{P}_{\mathrm{Ro}}$, and find that $\mathrm{Re} \propto \mathrm{Ra}^{0.47} \sim \mathrm{Ra}^{1/2}$ in the rota-

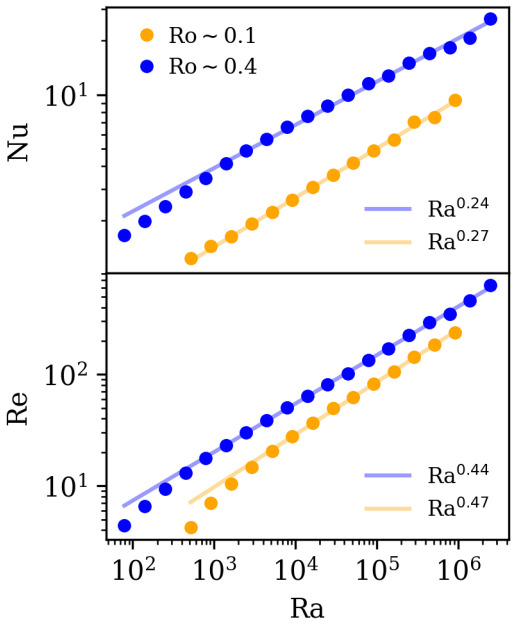

Figure 3. (a) Evolved Nu vs. Ra along constant $\mathcal{P}_{\rm Ro}$ paths. A scaling law of $\mathrm{Nu} \propto \mathrm{Ra}^{0.27}$ is observed, which is very similar to classic scaling laws. (b) Evolved Re vs. Ra along constant $\mathcal{P}_{\rm Ro}$ paths. A classic scaling law of $\mathrm{Re} \propto \mathrm{Ra}^{1/2}$ is observed. The similarity between these laws and classical laws in Rayleigh-Bénard convection suggests that at fixed $\mathcal{P}_{\rm Ro}$, varying Ra affects the evolved dynamics in a manner similar to a nonrotating fluid.

tionally constrained regime, which directly parallels the non-rotating regime in AB17.

In Fig. 4, we show time- and horizontally-averaged profiles of Ro and the entropy gradient (∇s). As Ra increases at a constant value of $\mathcal{P}_{\rm Ro}$, both the entropy and rotational boundary layers become thinner. We measure the thickness of the entropy boundary layer ($\delta_{\nabla s}$) at the top of the domain by fitting a line within the boundary layer and finding when that line crosses zero. We measure the thickness of the Ro boundary layer ($\delta_{\rm Ro}$) as the height of the peak value of Ro within upper half of the domain. In Fig. 4e, we plot $\delta_{\rm Ro}/\delta_{\nabla s}$, the ratio of these two boundary layers. As anticipated, the dynamical boundary layer ($\delta_{\rm Ro}$) becomes relatively thinner with respect to the thermal boundary layer ($\delta_{\nabla s}$) as Ro decreases. [Need a sentence saying what this means]

4. DISCUSSION

In this letter, we studied low-Mach-number, stratified, compressible convection under the influence of rotation. We examined three paths through Ra-Ta space, and showed that in the low-Ro, rotationally constrained regime, the newly-defined Predictive Rossby number, $\mathcal{P}_{\rm Ro} = \mathrm{Ra}/\mathrm{Ta}^{3/4}$, determines the value of the evolved Rossby number (Ro). While increasing Ra and holding $\mathcal{P}_{\rm Ro}$ constant, we find scaling laws of heat transport (Nu) and turbulence (Re) that are nearly identical to scaling laws seen in nonrotational convection.

Our results here suggest that experimenters can can achieve whatever degree of rotational constraint they desire in their evolved solution by choosing the proper value of $\mathcal{P}_{\rm Ro}$. Once that value is chosen, traditional experiments in which the turbulent nature of the solutions is increased by increasing the Ra can be straightforwardly achieved. Preliminary results in 3D spherical convective systems suggest that the results presented here are broadly applicable to rotational convection (Brown et al. 2019 in prep), even when the rotational vector is not every antiparallel to the gravity vector.

4.1. *acknowledgements*

EHA acknowledges the support of NASA NESSF (insert fellowship number) and the University of Colorado's George Ellery Hale Graduate Student Fellowship. This work was additionally supported by NASA LWS grant number NNX16AC92G. Computations were conducted with support by the NASA High End Computing (HEC) Program through the NASA Advanced Supercomputing (NAS) Division at Ames Research Center on Pleiades with allocations GID s1647.

REFERENCES

Anders, E. H., & Brown, B. P. 2017, Physical Review Fluids, 2, 083501

Augustson, K. C., Brown, B. P., Brun, A. S., Miesch, M. S., & Toomre, J. 2012, ApJ, 756, 169

Aurnou, J. M., & King, E. M. 2017, Proceedings of the Royal Society of London Series A, 473, 20160731

Brown, B. P., Browning, M. K., Brun, A. S., Miesch, M. S., & Toomre, J. 2008, ApJ, 689, 1354

—. 2010, ApJ, 711, 424

Brown, B. P., Miesch, M. S., Browning, M. K., Brun, A. S., & Toomre, J. 2011, ApJ, 731, 69

Brummell, N. H., Hurlburt, N. E., & Toomre, J. 1996, ApJ, 473, 494

—. 1998, ApJ, 493, 955

Busse, F. H. 2002, Physics of Fluids, 14, 1301

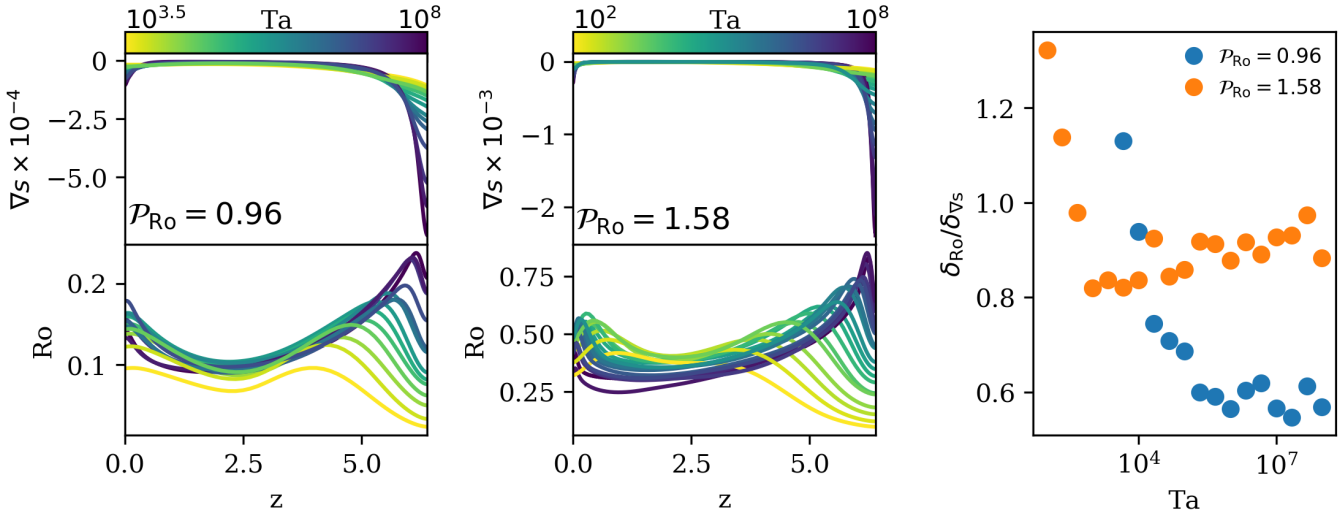

Figure 4. Horizontally-averaged profiles of the entropy gradient (∇s, a) and Rossby number (Ro, b) are shown vs. height for $\mathcal{P}_{\rm Ro} = 0.96$. Similar profiles are shown in (c) and (d) for $\mathcal{P}_{\rm Ro} = 1.58$. (c) The ratio of the sizes of the Ro boundary layer and ∇s boundary layer are shown. We find that for increasingly rotationally constrained flows, the Ro boundary layer is increasingly thinner than the thermal boundary layer.

Calkins, M. A., Julien, K., & Marti, P. 2015, Geophysical and Astrophysical Fluid Dynamics, 109, 422

Cheng, J. S., Stellmach, S., Ribeiro, A., et al. 2015, Geophysical Journal International, 201, 1

Featherstone, N. A., & Hindman, B. W. 2016, ApJ, 830, L15

Gastine, T., Wicht, J., & Aubert, J. 2016, Journal of Fluid Mechanics, 808, 690

Glatzmaier, G. A., & Gilman, P. A. 1982, ApJ, 256, 316

Greer, B. J., Hindman, B. W., & Toomre, J. 2016, ApJ, 824, 4

Guerrero, G., Smolarkiewicz, P. K., Kosovichev, A. G., & Mansour, N. N. 2013, ApJ, 779, 176

Julien, K., Knobloch, E., Rubio, A. M., & Vasil, G. M. 2012, Physical Review Letters, 109, 254503

Julien, K., Legg, S., McWilliams, J., & Werne, J. 1996, Journal of Fluid Mechanics, 322, 243

Käpylä, P. J., Käpylä, M. J., & Brandenburg, A. 2014, A&A, 570, A43

King, E. M., Stellmach, S., Noir, J., Hansen, U., & Aurnou, J. M. 2009, Nature, 457, 301

Soderlund, K. M., Sheyko, A., King, E. M., & Aurnou, J. M. 2015, Progress in Earth and Planetary Science, 2, 24

Stellmach, S., Lischper, M., Julien, K., et al. 2014, PhRvL, 113, 254501

Zhong, J.-Q., Stevens, R. J. A. M., Clercx, H. J. H., et al. 2009, Physical Review Letters, 102, 044502